TIME-RESOLVED OPTICAL SPECTROSCOPY AS A VERSATILE METHOD FOR STUDYING THE PHOTOTHERAPEUTIC ACTIVITY OF RUTHENIUM(II) COORDINATION COMPOUNDS

Cite this: *INEOS OPEN*, **2022**, *5 (3)*, 58–65
DOI: 10.32931/io2214r

Received 13 January 2023,
Accepted 13 February 2023

http://ineosopen.org

S. D. Tokarev* and A. Botezatu

Nesmeyanov Institute of Organoelement Compounds, Russian Academy of Sciences, ul. Vavilova 28, str. 1, Moscow, 119334 Russia

Abstract

Ruthenium(II) polypyridine complexes of imidazophenanthrolines are widely studied as photosensitizers for photodynamic therapy. The effectiveness of a therapeutic drug is manifested in its high cytotoxicity. Nowadays, the main methods for evaluating the drug effectiveness are still expensive and time-consuming photobiological studies on cell lines. It would be convenient to have access to simpler but no less reliable methods for evaluating the therapeutic efficacy. This review highlights recent investigations on the correlations between the photophysical behavior of ruthenium(II) complexes and their photobiological efficacy, as well as the possibilities of femto- and nanosecond time-resolved photophysical studies to establish the therapeutic efficacy.

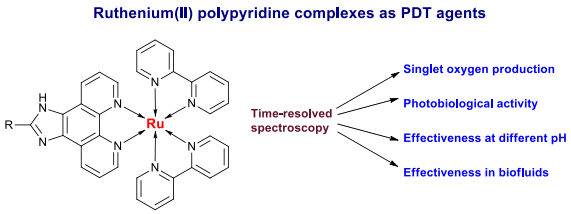

Key words: photodynamic therapy, transient absorption, time-resolved luminescence, ruthenium polypyridine complexes, phosphorescence.

Over the past three decades, imidazo[4,5-*f*][1,10]phenanthroline (imidazophenanthroline) and its derivatives (Scheme 1) have attracted considerable attention in different fields, including luminescent sensing, photodynamic therapy (PDT), photocatalysis, creation of organic light-emitting diodes (OLEDs) and molecular switches [1–5], as well as in medicine as DNA intercalators [6–10]. This is caused by two reasons: 1) the presence of a rigid and planar polyconjugated imidazophenanthroline core; 2) easy derivatization of the latter at the second position of the imidazole ring and the NH position. The properties of these compounds can readily be tuned depending on the intended application.

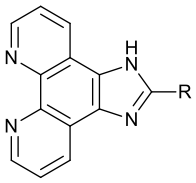

Scheme 1

The nitrogen atoms of the 1,10-phenathroline core can serve as convenient coordination sites for a large series of d- and f-elements. Therefore, imidazophenanthroline derivatives are often considered as sensors for metal cations [11–13] and ligands for functional metal complexes. Among different central cations in imidazophenanthroline complexes, Ru(II) is the most popular one. The main advantage of these complexes is their electronic structure which ensures absorption in the visible region of light with the formation of a long-lived excited triplet state capable of injecting an electron into many organic and inorganic acceptors. They also exhibit high chemical and photoresistance. Ruthenium(II) complexes of imidazophenanthrolines are among the most common metal-based photosensitizers; the most significant advances in this field are covered annually in several reviews [14–16]. The traditional application scope of ruthenium(II) imidazophenanthroline complexes as photosensitizers includes photocatalysis [17, 18], dye-sensitized solar cells [19–21], and photodynamic therapy (PDT) of cancer [22–27]. Our recent review also highlighted the use of these complexes as pH sensors, oxygen sensors, and photosensitizers for semiconductor gas sensors [28].

Among the mentioned application fields of ruthenium(II) imidazophenanthroline complexes, PDT is most urgent, widely explored, and close to the practical application. PDT is aimed at destroying cancer cells with reactive oxygen species (ROS) under the action of light. ROS are formed as a result of the activation of a special substance, a photosensitizer, with light and the subsequent transfer of activation energy to the ROS sources. This type of therapy is accomplished by the synergistic action of three components: a photosensitizer (PS), molecular oxygen, and light (usually visible light), which are individually harmless.

The PS can be injected both locally and into the bloodstream; then the treatment area is irradiated with the light of the appropriate wavelength [15]. The PS undergoes a transition from a ground state to an excited singlet state ^{1}PS*

and then, as a result of intersystem crossing, to an excited triplet state ^{3}PS* which interacts directly or indirectly with molecular oxygen according to the following two basic mechanisms.

- In the first mechanism, the excited triplet state ^{3}PS* and surrounding biomolecules exchange an electron or a proton to form highly reactive short-lived (about 1 ns) radicals that react with water or molecular oxygen to form ROS destroying the cell (for example, superoxide anion $O_2^{\bullet-}$, hydroxyl radical $OH^{\bullet}$, or hydrogen peroxide H_2O_2);
- In the second mechanism, the excited triplet state ^{3}PS* directly transfers energy to molecular oxygen in its ground triplet state ($^3O_2$) to form singlet oxygen ($^1O_2$). The latter has a lifetime of no more than 40 ns in a biological environment [29] and is one of the most effective cytotoxic reagents used in therapy.

There is also a third oxygen-independent mechanism. Its therapeutic effect is associated with the elimination of one of the ligands upon PS photoexcitation and subsequent chelation of ruthenium(II) cations by biomolecules. As a result, the latter lose their functionality and a cytotoxic effect is achieved. This mechanism has been studied to a lesser extent but it has great potential since the therapeutic effect is achieved even under hypoxic conditions [30].

However, the first two mechanisms associated with the formation of ROS or singlet oxygen are the main ones in both research and practice. The PS efficiency, even in the first approximation, depends on a significant number of parameters: accumulation in the tumor, low dark toxicity, the ability to absorb light in the therapeutic window (620–850 nm), as well as the possibility of transition to a triplet excited state and its lifetime.

One of the best results is currently demonstrated by the polypyridine complex TLD1433 (Scheme 2).

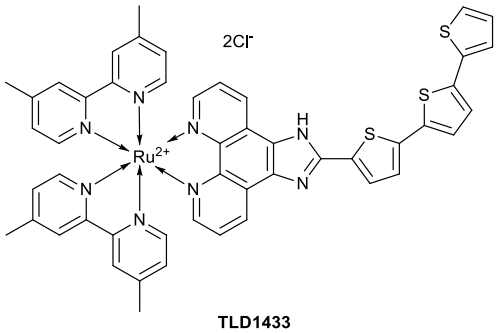

TLD1433

Scheme 2

Fong *et al*. [31] reported the results of *in vivo* experiments on BALB/c mice using TLD1433 and selected the optimal conditions for therapy. Thus, irradiation of the tumor after the drug administration with green light (525 nm, 192 J/cm^2, 200 mW/cm^2) led to complete regression of the neoplasm within 10 days. In the next work, this research group used the same PS in combination with longer wavelength light [32]. Despite the high penetrating ability of near-IR light into tissues, they failed to reach acceptable values of *in vivo* toxicity towards cancer cells. This is likely to be associated with the low values of the PS extinction coefficient at the irradiation wavelength. However, the authors proposed an original method for increasing the efficiency of PDT using IR radiation—the application of TLD1433 associates with transferrin. The addition of transferrin provided high photostability, the ability to absorb near-IR light, and selective delivery to cancer cells.

Currently, TLD1433 is one of four metal-based photosensitizers approved for use in PDT in humans and is undergoing the second stage clinical trials [33]. The detailed reviews on the application of ruthenium(II) polypyridine complexes in PDT are published almost every year [34–37].

In vitro and *in vivo* studies are expensive and time-consuming. As a rule, the investigation of new PSs begins with the photophysical characteristics of the molecule since they determine the fundamental possibility of using the complex as a PDT agent. The transition to a triplet excited state in the case of imidazophenanthroline polypyridine complexes of ruthenium(II) is provided by the heavy central cation; however, the characteristic lifetimes of their excited states in degassed solutions are about 1 μs, which may be insufficient. The HOMO in these complexes is localized mainly on the central cation, while the LUMO is localized on ligands; therefore, the transition from the ground state is called metal-to-ligand charge transfer (MLCT), and the corresponding triplet excited state is designated as ^{3}MLCT. It is assumed that the longer its lifetime, the more likely the energy transfer to neighboring molecules in the cell, which means the higher the therapeutic effect.

To increase the lifetime of the ^{3}MLCT state, Stephenson *et al.* [38] introduced a pyrene moiety into the structure of the imidazophenanthroline-based ligand (Scheme 3). As a result, a new intraligand (IL) electronic transition appeared in the absorption spectrum of **1**, which forms an excited triplet state ^{3}IL localized on the pyrene unit. The energy of ^{3}IL is slightly lower than that of ^{3}MLCT (by no more than 0.1 eV), which leads to a redistribution of the excitation energy between these states, deceleration of phosphorescence, and, as a result, to a significant lifetime of the ^{3}MLCT state. Reichardt, McFarland, and colleagues published a series of reports devoted to ruthenium PSs for PDT [39–42]. A distinctive feature of these works is the extensive use of photophysical experiments (time-resolved luminescence and transient absorption spectroscopy) to establish the dynamics of excited states, which dictates the effectiveness of therapy—the main biomedical characteristic of a PDT agent.

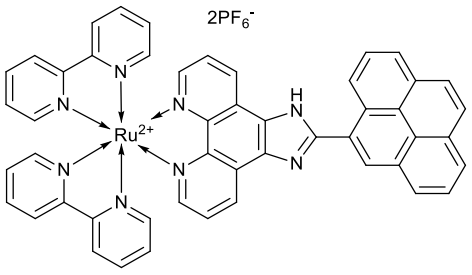

1

Scheme 3

Stephenson *et al.* [38] demonstrated high cytotoxicity of the proposed structure against human leukemia cancer cells upon irradiation with light. The PDT agents are evaluated based on three parameters: the values of EC_{50} (effective concentration necessary to reduce cell viability to 50%) in the dark and upon irradiation, as well as the phototherapeutic index (PI), PI = EC_{50}

(dark)/EC_{50} (light). The proposed structure features the following characteristics: EC_{50} (dark) = 165 μM, EC_{50} (light) = 400 nM, and PI = 413 towards human promyelocytic leukemia cell line (HL-60) when irradiated with full-spectrum visible light. The effectiveness of new metal-based PSs for PDT is often compared to that of the widely used chemotherapeutic agent cisplatin (*cis*-[$Pt(NH_3)_2Cl_2$]). This drug is not photoactive—its cytotoxic effect is based on the ligand exchange with DNA in the cell, which leads to its apoptosis. The value of EC_{50} for cisplatin towards HL-60 cells ranges within 3–6 μM depending on the incubation time [43]. Thus, PS **1** is 50–30 times safer in the dark than the clinically used drug. However, when the area of PS concentration is exposed to light, its cytotoxic effect exceeds that of cisplatin by 10 times. This clearly indicates the advantages of PDT over chemotherapy: the overall non-toxicity with the increased efficiency in the area of light exposure. The efficiency of **1** also extends to biofilms, dense colonies of bacteria, where its concentration of only 10 nM was enough to kill 75% of the bacterial population. The results of this study demonstrate the versatility of **1** in killing both cancerous and bacterial cells and expand the scope of metal complexes that have low-lying ^{3}ILs for photobiological applications.

Subsequently the same research group [44] used nanosecond transient absorption and time-resolved luminescence spectroscopy to determine the number of excited states and their lifetimes. The kinetics of recovery of the transient absorption allowed the authors to calculate the nonradiative relaxation lifetime: 50 μs (Fig. 1A). The emission decay kinetics showed two radiative lifetimes, 0.6 and 26 μs, which correspond to spontaneous and delayed phosphorescence (Fig. 1B). The deceleration is accomplished due to the equilibrium between emitting ^{3}MLCT state and non-emitting ^{3}IL level lying lower in energy.

Then using transient absorption spectroscopy on femtosecond scale, the existence of two processes with lifetimes of 3 and 39 ps was demonstrated. The faster process was associated with the vibrational relaxation of the ^{3}MLCT state, while the second one, according to the authors, relates to the rotation of the pyrene moiety relative to the imidazophenanthroline unit for the formation of the ^{3}IL. To confirm this assumption, the femtosecond transient absorption kinetics was studied depending on the medium density. Figures 2A and 2B show the transient absorption spectra (at 1 and 100 ps) after photoexcitation and transient absorption traces at 560 nm in four different solvents, respectively. In each case, the experimental transient absorption growth kinetics were approximated by two lifetimes. As expected, the longer lifetime correlated with the medium viscosity and also inversely depended on the solvent polarity (Fig. 2C). More polar solvents (*e.g.*, DMSO) better compensate for the dipole state formed during the transition of an electron from the metal cation to the remote pyrene moiety, and therefore facilitate the transition to this state and reduce the characteristic transition time.

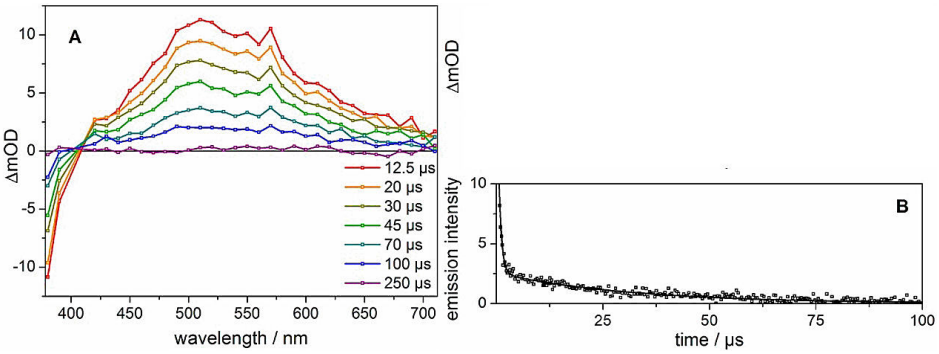

Figure 1. Nanosecond transient absorption spectra recorded for **1** in water upon pumping at 410 nm at different delay times (**A**). Emission decay kinetics recorded for **1** in water at 600 nm pumping at 410 nm (**B**). (Reprinted with permission from C. Reichardt *et al.*, *J. Phys. Chem. A*, **2015**, *119*, 3986–3994. DOI: 10.1021/acs.jpca.5b01737. Copyright (2015) American Chemical Society)

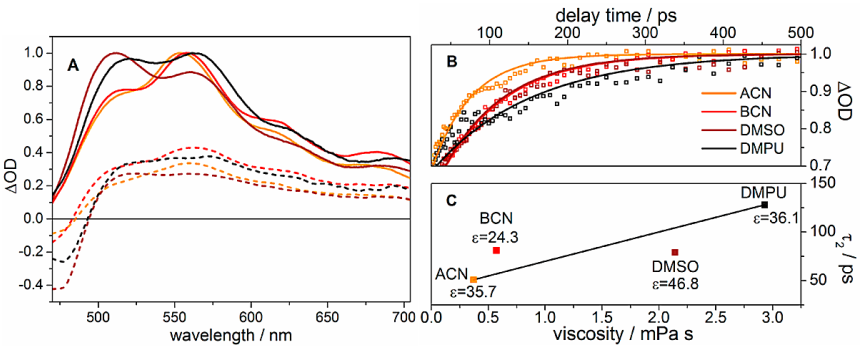

Figure 2. Transient absorption data collected for **1** (λ_{pump} = 403 nm) in acetonitrile (ACN) (orange), butyronitrile (BCN) (red), dimethylsulfoxide (DMSO) (brown), and 1,3-dimethyl-3,4,5,6-tetrahydro-2(1H)-pyrimidinone (DMPU) (black). Transient absorption spectra at 1 (dashed line) and 100 ps (solid line) normalized to the maximum positive ΔOD signal of the 100 ps spectra (**A**). Transient absorption traces at 560 nm for all solvents (**B**). Symbols represent experimental data, while solid lines refer to the curve obtained from the global fit. The kinetic traces are normalized to the maximum ΔOD signal at long delay times. Dependence of τ_2 on the viscosity and polarity of the solvents (**C**). (Reprinted with permission from C. Reichardt *et al.*, *J. Phys. Chem. A*, **2015**, *119*, 3986–3994. DOI: 10.1021/acs.jpca.5b01737. Copyright (2015) American Chemical Society)

Hence, time-resolved spectroscopy techniques allowed for establishing the main processes that occur during photoexcitation of **1** in neutral aqueous solutions and also showed their effectiveness in model cell systems. The resulting Jablonski diagram for **1** in an aqueous solution is depicted in Fig. 3.

PS **1** contains an imidazole moiety sensitive to pH. The protonation or deprotonation of this unit can have a strong effect on the excited states at physiological pH values and can also provide additional selectivity to the PS towards the cells featuring pH abnormalities due to metabolic changes. Reichardt *et al.* [45] studied the effect of protonation on the dynamics of excited states and, consequently, the physiological activity of **1**. The research objects were three aqueous solutions with a predominant content of the neutral (designated as RuH), protonated (RuH_2), and deprotonated (Ru) imidazole rings. The mentioned forms of **1** were obtained *in situ* by adjusting the pH value with a strong acid or base. As expected, the changes in the protonation state of the imidazole unit affected the electronic nature of the excited state.

The picosecond dynamics of the protonated form RuH_2 was found to be similar to that of neutral RuH and included ^{3}MLCT vibrational relaxation (τ_1 = 1.6 ps) and subsequent rotation of the pyrene moiety relative to the imidazole system (τ_2 = 18 ps) (Fig. 4A). Additionally, a process was observed that was associated with the fast reverse energy transfer from the ^{3}IL state to the ^{3}MLCT one (τ_3 = 195 ps), which was not detected in the case of RuH. The lifetimes of spontaneous and delayed phosphorescence during protonation changed only slightly (τ_{em1} = 0.9 μs, τ_{em1} = 24 μs for RuH and τ_{em1} = 0.6 μs, τ_{em1} = 26 μs for RuH_2), and the nonradiative relaxation time with ^{3}IL also remained unchanged (τ_3 = 52 μs). This implies that **1** is equally effective as a photosensitizer in neutral and protonated forms (Figs. 4B and 4C). In the case of the deprotonated form Ru, only spontaneous phosphorescence from the ^{3}MLCT state was detected (τ_{em1} = 0.6 μs). The absence of delayed emission suggests that the energy gap between the ^{3}MLCT and ^{3}IL states is larger than that for RuH and RuH_2. In the picosecond region, a process of energy transfer from the ^{3}MLCT state to the ^{3}IL one with the lifetime of τ_3 = 830 ps was revealed. This also indicates a significant difference in the energy of the ^{3}MLCT and ^{3}IL states, which prohibits delayed emission (Fig. 4D).

Thus, the highly photosensitizing ^{3}IL states can be achieved by changing the protonation state of the imidazole moiety. The charge of a therapeutic molecule can significantly affect its cellular uptake, localization, and affinity for certain biological targets. It is also known that some ruthenium(II) complexes exhibit pH-dependent DNA binding. This opens the way to an additional mechanism for controlling the PDT selectivity towards some unhealthy cells by the pH-dependent population of the ^{3}IL states and PS charge control.

In the next work, Reichardt *et al.* [46] adjusted the properties of model research systems closer to the real ones by selecting the optimal parameters of the environment. The photophysical behavior of **1** was studied in a simulated body fluid (SBF) with high ionic strength, a more physiologically suitable solvent that contains a complex mixture of ions at pH 7.4. The femtosecond studies revealed an additional process occurring in the photoexcited state (τ_3 = 764 ps). It was assumed to be caused by the interaction of the highly concentrated ions

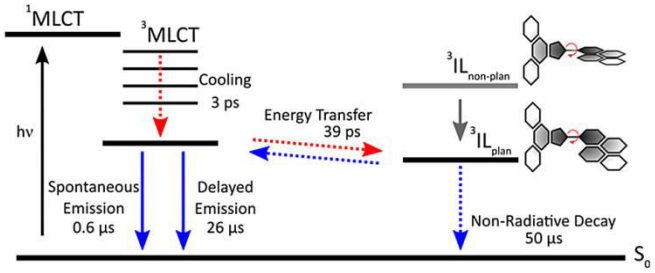

Figure 3. Jablonski diagram representing the established photophysics of **1** in water. Red and blue arrows indicate processes on the picosecond and microsecond time scales, respectively. Corresponding time constants obtained by freeze–pump–thaw degassing. (Reprinted with permission from C. Reichardt *et al.*, *J. Phys. Chem. A*, **2017**, *121*, 5635–5644. DOI: 10.1021/acs.jpca.7b04670. Copyright (2017) American Chemical Society)

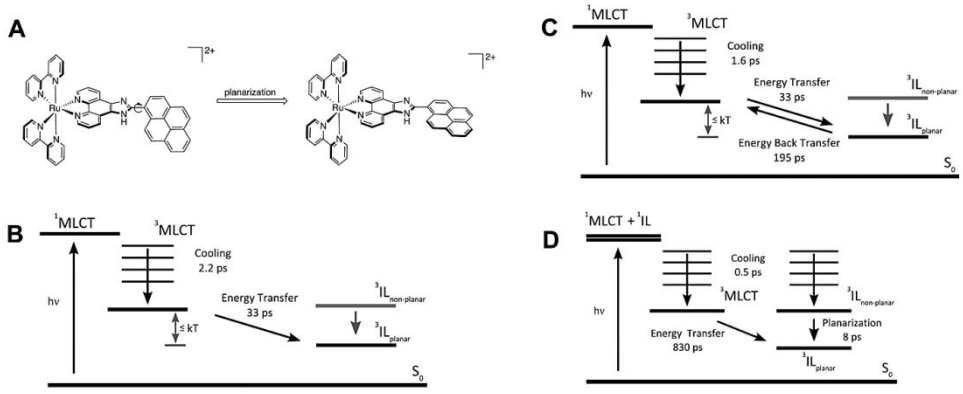

Figure 4. Structures of the non-planar and planar ^{3}IL state (**A**). Jablonski schemes of the three protonation states RuH (**B**), RuH_2 (**C**), and Ru (**D**) based on the femtosecond transient absorption experiments upon excitation at 403 nm. (Reprinted with permission from C. Reichardt *et al.*, *J. Phys. Chem. A*, **2016**, *120*, 6379–6388. DOI: 10.1021/acs.jpca.6b05957. Copyright (2016) American Chemical Society)

with the imidazophenanthroline ligand. This process was observed in high ionic strength SBF but was not observed in water, simple buffers, or low ionic strength SBF. The dynamics of the photoinduced states was also studied in an aqueous solution of DNA. In the presence of the biomolecule, the rotation of the pyrene moiety relative to the imidazophenanthroline unit for the formation of the ^{3}IL state appeared to be accelerated (from 39 to 18 ps). The increased rate of coplanarization of the pyrene and imidazole units was associated with the intercalation of **1** into the DNA molecule, which leads to conformational restrictions on the rotation of the pyrene moiety relative to the imidazole unit. Furthermore, in the presence of DNA, the lifetimes of delayed phosphorescence and nonradiative relaxation of the ^{3}IL were equalized (37.5 and 40 μs, respectively). The authors suggested the presence of two close but different ^{3}IL excited states for **1**, both with coplanar pyrene and imidazophenanthroline units (Fig. 5C). These states differ in the overlapping with the ^{3}MLCT state and, consequently, in the probability of mutual energy transfer with this level. In an aqueous solution (as well as in a buffer solution with pH 7.4 and SBF with pH 7.4), one of them is responsible for delayed phosphorescence (green arrow in Fig. 5A), while the second one (characterized by a lower probability of interaction with ^{3}MLCT) leads to nonradiative relaxation (blue arrow in Fig. 5A). During intercalation, **1** loses its conformational mobility, and one of the ^{3}IL states becomes inaccessible (Fig. 5B), while the remaining one participates in equiprobable processes of delayed phosphorescence and nonradiative relaxation, which causes the equality of their lifetimes.

The photobiological activity of PSs such as **1** is ultimately determined by the nature and lifetimes of excited states as well as the deactivation channels. Therefore, defining the state responsible for photobiological activity and then establishing the effect of biological parameters on this state are urgent tasks. The considered work emphasizes the importance of investigations on the models close to the real systems and the convenience of photophysical methods for this purpose.

However, the research group of Prof. Reichardt went further and reported the results of *in cellulo* study of ultrafast excitation processes using time-resolved spectroscopy [47]. The widely studied phenazine-containing complex **2** was chosen as a main research object (Scheme 4).

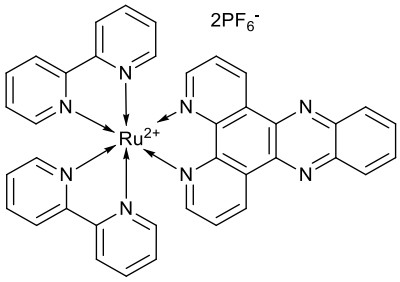

2

Scheme 4

The experiments were carried out on HepG2 cancer cells. They were incubated with a solution of complex **2**, fixed on a substrate, and studied using a special device which combined laser scanning microscopy with pump-probe spectroscopy. This unit was called a transient absorption microscope.

Using emission microscopy, the authors confirmed the localization of **2** in the nuclei of HepG2 cells where the PS interacts with DNA. The results of time-resolved studies *in cellulo* showed characteristic photoinduced picosecond dynamics of **2**, which, however, seems to depend on the cellular localization. Unfortunately, the experimental conditions may lead to cell damage. This means that DNA fragments can enter the intracellular compartment where they can interact with **2** under various conditions. Nevertheless, this is a pioneering work that demonstrated for the first time the possibility of application of picosecond photophysical methods for investigation of the behavior of PS in a cell. This approach brings laboratory biochemical and physical studies as close as possible to the biomedical application of future PDT agents. The results obtained show the necessity and possibility of exploring the photoinduced processes of coordination compounds for intracellular use in a real target biological environment.

In the latest work on ruthenium-containing PSs, Reichardt, McFarland, and co-workers [48] studied the correlations between photocytotoxicity and photophysical data. The previous

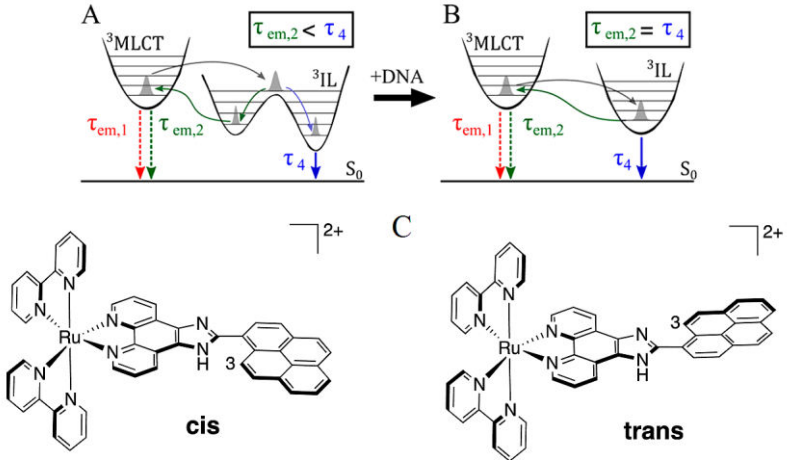

Figure 5. Jablonski diagrams of the deactivation pathways in the nanosecond time regime for **1** in water, Tris–HCl/NaCl buffer solution, or SBF (**A**) or in Tris–HCl/NaCl containing salmon sperm DNA (**B**). Two possible conformations of **1** (after planarization on the ultrafast time scale) that give rise to the double potential of the ^{3}IL state (**C**). (Reprinted with permission from C. Reichardt *et al.*, *J. Phys. Chem. A*, **2017**, *121*, 5635–5644. DOI: 10.1021/acs.jpca.7b04670. Copyright (2017) American Chemical Society)

reports demonstrated the importance of the low-lying ^{3}IL level for increasing the lifetime of the excited state. It was hypothesized that the lifetime of the excited state is proportional to the photocytotoxicity. However, to establish a reliable correlation, it is necessary to study a set of PSs with a large spread in the lifetimes of the excited state. The authors selected eight complexes of ruthenium and osmium **f1**–**f8** which differ markedly in the configuration of the triplet state and lifetime (Scheme 5).

For each PS, the following parameters were determined: the luminescence lifetime, nonradiative lifetime, ROS production efficiency, singlet oxygen quantum yield, and the values of EC_{50} on human melanoma cells SKMEL28 and human leukemia cells HL60 upon two types of irradiation (broadband white and monochromatic red light) and in the dark.

A strong correlation between the photobiological activity and ROS production efficiency was revealed. The production of ROS is directly proportional to the lifetime of the triplet excited state and singlet oxygen quantum yield. Compounds **f1**–**f3**, **f5** with the lifetimes of nonradiative relaxation of 22.9, 14.2, 17.1, and 12.1 μs, respectively, proved to be effective PDT agents with the high cytotoxic activity in the light, even when irradiated with red light for which the extinction coefficients are very low, as well as the low dark cytotoxicity. On the contrary, compounds **f4**, **f6**–**f8** with the lifetimes of less than 1 μs appeared to be significantly less active. It is worth noting that, under other conditions being equal, osmium complex **f4** features a much lower values of PI than its ruthenium analog **f1**. The use of a heavier metal results in the lower ^{3}MLCT energy and greater spin–orbit coupling (SOC). This leads to a decrease in the lifetime of the excited state, which in turn reduces the efficiency of ROS generation. Nevertheless, the key advantage of **f4** over **f1** is the ability to absorb light in the biological window, which makes these osmium complexes promising objects for further studies as PDT agents. It is important to note that the photophysical parameters determined in an acetonitrile solution turned out to be reliable indicators of the aqueous photobiological activity. This simplifies the search for promising photobiological agents.

The authors plotted a number of two-dimensional correlations of the parameters determined and then proposed the use of three-dimensional maps in the coordinates ROS production–Transient absorption lifetime–Photocytotoxicity. In different cases, different parameters of cytotoxicity are important. For example, for a tumor-selective PDT agent, the best characteristic is EC_{50} since it is quickly accumulated only in the tumor and does not have time to significantly harm the body (Fig. 6A). For a non-selective PS, the phototherapeutic index PI comes to the fore. It is important for the PS which is evenly distributed throughout the body to exert the cytotoxic effect only in the area of irradiation, so its PI must be as high as possible (Fig. 6B).

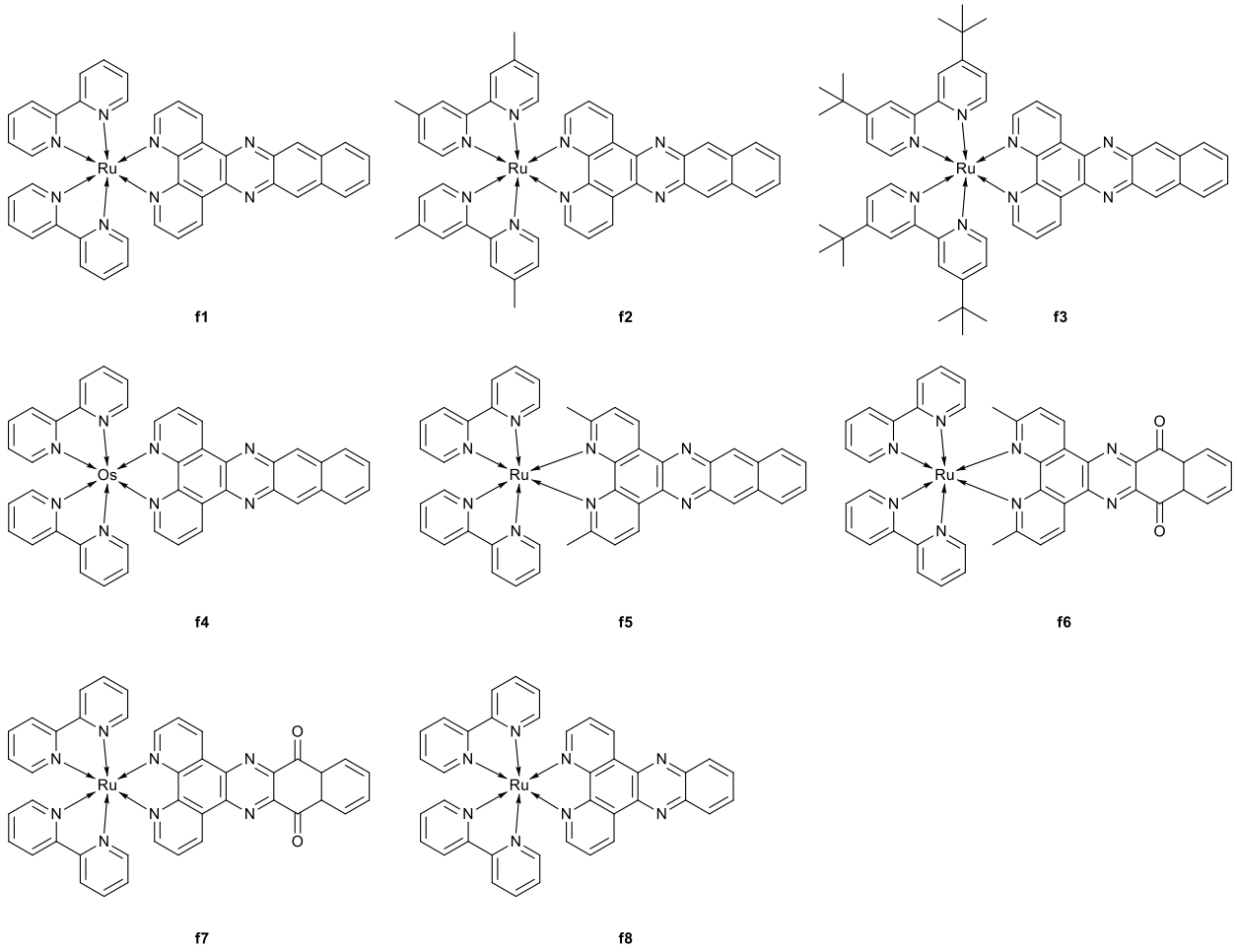

Scheme 5

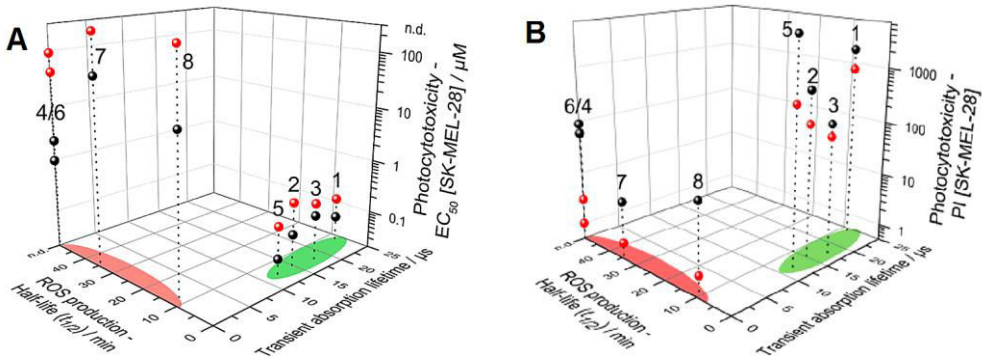

Figure 6. Correlation between the transient absorption lifetime, half-life from the ROS assay, and *in vitro* EC_{50} values (**A**) or PI values (**B**) for complexes **f1**–**f8** in SK-MEL-28 cells after irradiation with visible (black) or red (red) light. The green and red areas show the classification of the compounds as effective or ineffective photobiological agents, respectively. (Reprinted with permission from C. Reichardt *et al.*, *Inorg. Chem.*, **2019**, *68*, 3156–3166 (Supporting Information). DOI: 10.1021/acs.inorgchem.8b03223. Copyright (2019) American Chemical Society)

The works discussed above show great potential of transient absorption spectroscopy for establishing the efficacy of coordination compounds with a triplet excited state as PDT agents. The optical methods revealed significant differences in the photophysical behavior of the studied compounds in simple solutions and model biological media SBF. Nevertheless, it was demonstrated that the efficiency of the metal-based PSs can be evaluated in the first approximation in a photophysical laboratory without recourse to time-consuming biological experiments. Many current reviews conclude that, although most of the Ru(II) polypyridine complexes bearing various ligands were characterized and studied *in vitro*, there is a lack of knowledge about their biological and metabolic characteristics. As shown above, modern instrumentation for time-resolved photophysical studies gives an opportunity to look into the cell and enables the investigations on the PS behavior in the biological environment. Nevertheless, there are a number of important physical and biological issues that need to be resolved for wider application of ruthenium(II) polypyridine complexes in PDT: an increase in the PS absorption in the biological window due to the red shift of the MLCT band or an increase in the probability of two-photon absorption; targeted delivery of this type of PSs to the tumor; determination of PS metabolism before and after therapy.

Acknowledgements

This work was performed within the State Task of the Ministry of Science and Higher Education of the Russian Federation (topic no. FFSF-2022-0017).

Corresponding author

* E-mail: tokarev@ineos.ac.ru (S. D. Tokarev)

References

1. R.-Y. Wang, W.-L. Jia, H. Aziz, G. Vamvounis, S. Wang, N.-X. Hu, Z. D. Popović, J. A. Coggan, *Adv. Funct. Mater.*, **2005**, *15*, 1483–1487. DOI: 10.1002/adfm.200500041
2. S. Xiao, T. Yi, Y. Zhou, Q. Zhao, F. Li, C. Huang, *Tetrahedron*, **2006**, *62*, 10072–10078. DOI: 10.1016/j.tet.2006.08.061
3. J.-F. Lee, Y.-C. Chen, J.-T. Lin, C.-C. Wu, C.-Y. Chen, C.-A. Dai, C.-Y. Chao, H.-L. Chen, W.-B. Liau, *Tetrahedron*, **2011**, *67*, 1696–1702. DOI: 10.1016/j.tet.2010.12.059
4. J. Peng, J. Sun, P. Gong, P. Xue, Z. Zhang, G. Zhang, R. Lu, *Chem. Asian J.*, **2015**, *10*, 1717–1724. DOI: 10.1002/asia.201500299
5. J. Jayabharathi, V. Thanikachalam, M. V. Perumal, *Spectrochim. Acta, Part A*, **2012**, *85*, 31–37. DOI: 10.1016/j.saa.2011.08.060
6. C.-Y. Wei, J.-H. Wang, Y. Wen, J. Liu, L.-H. Wang, *Bioorg. Med. Chem.*, **2013**, *21*, 3379–3387. DOI: 10.1016/j.bmc.2012.11.059
7. L. Wang, Y. Wen, J. Liu, J. Zhou, C. Li, C. Wei, *Org. Biomol. Chem.*, **2011**, *9*, 2648–2653. DOI: 10.1039/C0OB00961J
8. S. Liao, Z. Zhang, Q. Wu, X. Wang, W. Mei, *Bioorg. Med. Chem.*, **2014**, *22*, 6503–6508. DOI: 10.1016/j.bmc.2014.09.003
9. N. Zhen, Q. Yang, Q. Wu, X. Zhu, Y. Wang, F. Sun, W. Mei, Y. Yu, *Cancer Chemother. Pharmacol.*, **2016**, *77*, 169–180. DOI: 10.1007/s00280-015-2894-5
10. L. Li, J.-Q. Cao, H.-M. Liu, Q. Wu, Q.-H. Pan, Z.-P. Zeng, Y.-T. Lan, Y.-M. Li, W.-J. Mei, X.-C. Wang, W.-J. Zheng, *Molecules*, **2017**, *22*, 829. DOI: 10.3390/molecules22050829
11. Y. Sotnikova, E. Lukovskaya, A. Bobylyova, Y. Fedorov, V. Novikov, A. Peregudov, A. Anisimov, A. D'Aleo, F. Fages, O. Fedorova, *Inorg. Chim. Acta*, **2016**, *445*, 103–109. DOI: 10.1016/j.ica.2016.02.029
12. X. Zhang, L.-l. Li, Y.-k. Liu, *Mater. Sci. Eng. C*, **2016**, *59*, 916–923. DOI: 10.1016/j.msec.2015.10.080
13. Z.-B. Zheng, Z.-M. Duan, J.-X. Zhang, K.-Z. Wang, *Sens. Actuators, B*, **2012**, *169*, 312–319. DOI: 10.1016/j.snb.2012.05.003
14. S. Kumar, S. Singh, A. Kumar, K. S. R. Murthy, A. K. Singh, *Coord. Chem. Rev.*, **2022**, *452*, 214272. DOI: 10.1016/j.ccr.2021.214272
15. L. Conti, E. Macedi, C. Giorgi, B. Valtancoli, V. Fusi, *Coord. Chem. Rev.*, **2022**, *469*, 214656. DOI: 10.1016/j.ccr.2022.214656
16. J. Mo, N. P. M. Le, R. Priefer, *Eur. J. Med. Chem.*, **2021**, *225*, 113770. DOI: 10.1016/j.ejmech.2021.113770
17. N. Queyriaux, E. S. Andreiadis, S. Torelli, J. Pecaut, B. S. Veldkamp, E. A. Margulies, M. R. Wasielewski, M. Chavarot-Kerlidou, V. Artero, *Faraday Discuss.*, **2017**, *198*, 251–261. DOI: 10.1039/C6FD00204H
18. R. V. Khade, S. D. Choudhury, H. Pal, A. S. Kumbhar, *ChemPhysChem*, **2018**, *19*, 2380–2388. DOI: 10.1002/cphc.201800313
19. C.-Y. Chen, H.-C. Lu, C.-G. Wu, J.-G. Chen, K.-C. Ho, *Adv. Funct. Mater.*, **2007**, *17*, 29–36. DOI: 10.1002/adfm.200600059
20. D. Kuang, C. Klein, S. Ito, J.-E. Moser, R. Humphry-Baker, N. Evans, F. Duriaux, C. Grätzel, S. M. Zakeeruddin, M. Grätzel, *Adv. Mater.*, **2007**, *19*, 1133–1137. DOI: 10.1002/adma.200602172

21. J.-K. Lee, M. Yang, *Mater. Sci. Eng. B*, **2011**, *176*, 1142–1160. DOI: 10.1016/j.mseb.2011.06.018
22. S. Li, J. Zhao, X. Wang, G. Xu, S. Gou, Q. Zhao, *Inorg. Chem.*, **2020**, *59*, 11193–11204. DOI: 10.1021/acs.inorgchem.0c01860
23. G. Ghosh, K. L. Colón, A. Fuller, T. Sainuddin, E. Bradner, J. McCain, S. M. A. Monro, H. Yin, M. W. Hetu, C. G. Cameron, S. A. McFarland, *Inorg. Chem.*, **2018**, *57*, 7694–7712. DOI: 10.1021/acs.inorgchem.8b00689
24. F. J. Ballester, E. Ortega, D. Bautista, M. D. Santana, J. Ruiz, *Chem. Commun.*, **2020**, *56*, 10301–10304. DOI: 10.1039/d0cc02417a
25. S. Banerjee, *ChemBioChem*, **2021**, *22*, 2407–2409. DOI: 10.1002/cbic.202100102
26. C. Mari, V. Pierroz, S. Ferrari, G. Gasser, *Chem. Sci.*, **2015**, *6*, 2660–2686. DOI: 10.1039/c4sc03759f
27. J. Karges , S. Kuang, F. Maschietto, O. Blacque, I. Ciofini, H. Chao, G. Gasser, *Nat. Commun.*, **2020**, *11*, 3262. DOI: 10.1038/s41467-020-16993-0
28. S. D. Tokarev, Yu. V. Fedorov, *INEOS OPEN*, **2020**, *3*, 55–65. DOI: 10.32931/io2010r
29. A. P. Castano, T. N. Demidova, M. R. Hamblin, *Photodiagn. Photodyn. Ther.*, **2005**, *2*, 1–23. DOI: 10.1016/S1572-1000(05)00030-X
30. J. A. Roque III, H. D. Cole, P. C. Barrett, L. M. Lifshits, R. O. Hodges, S. Kim, G. Deep, A. Francés-Monerris, M. E. Alberto, C. G. Cameron, S. A. McFarland, *J. Am. Chem. Soc.*, **2022**, *144*, 8317–8336. DOI: 10.1021/jacs.2c02475
31. J. Fong, K. Kasimova, Y. Arenas, P. Kaspler, S. Lazic, A. Mandel, L. Lilge, *Photochem. Photobiol. Sci.*, **2015**, *14*, 2014–2023. DOI: 10.1039/c4pp00438h
32. P. Kaspler, S. Lazic, S. Forward, Y. Arenas, A. Mandel, L. Lilge, *Photochem. Photobiol. Sci.*, **2016**, *15*, 481–495. DOI: 10.1039/c5pp00450k
33. https://clinicaltrials.gov/ct2/show/NCT03053635.
34. F. Heinemann, J. Karges, G. Gasser, *Acc. Chem. Res.*, **2017**, *50*, 2727–2736. DOI: 10.1021/acs.accounts.7b00180
35. J. Liu, C. Zhang, T. W. Rees, L. Ke, L. Ji, H. Chao, *Coord. Chem. Rev.*, **2018**, *363*, 17–28. DOI: 10.1016/j.ccr.2018.03.002
36. M. Martínez-Alonso, G. Gasser, *Coord. Chem. Rev.*, **2021**, *434*, 213736. DOI: 10.1016/j.ccr.2020.213736
37. Y. Wu, S. Li, Y. Chen, W. He Z. Guo, *Chem. Sci.*, **2022**, *13*, 5085–5106. DOI: 10.1039/D1SC05478C
38. M. Stephenson, C. Reichardt, M. Pinto, M. Wächtler, T. Sainuddin, G. Shi, H. Yin, S. Monro, E. Sampson, B. Dietzek, S. A. McFarland, *J. Phys. Chem. A*, **2014**, *118*, 10507–10521. DOI: 10.1021/jp504330s
39. S. Monro, K. L. Colón, H. Yin, J. Roque III, P. Konda, S. Gujar, R. P. Thummel, L. Lilge, C. G. Cameron, S. A. McFarland, *Chem. Rev.*, **2019**, *119*, 797–828. DOI: 10.1021/acs.chemrev.8b00211
40. S. A. McFarland, A. Mandel, R. Dumoulin-White, G. Gasser, *Curr. Opin. Chem. Biol.*, **2020**, *56*, 23–27. DOI: 10.1016/j.cbpa.2019.10.004
41. G. Shi, S. Monro, R. Hennigar, J. Colpitts, J. Fong, K. Kasimova, H. Yin, R. DeCoste, C. Spencer, L. Chamberlain, A. Mandel, L. Lilge, S. A. McFarland, *Coord. Chem. Rev.*, **2015**, *282*, 127–138. DOI: 10.1016/j.ccr.2014.04.012
42. L. M. Lifshits, J. A. Roque III, P. Konda, S. Monro, H. D. Cole, D. von Dohlen, S. Kim, G. Deep, R. P. Thummel, C. G. Cameron, S. Gujar, S. A. McFarland, *Chem. Sci.*, **2020**, *11*, 11740–11762. DOI: 10.1039/D0SC03875J
43. T. Sainuddin, M. Pinto, H. Yin, M. Hetu, J. Colpitts, S. A. McFarland, *J. Inorg. Biochem.*, **2016**, *158*, 45–54. DOI: 10.1016/j.jinorgbio.2016.01.009
44. C. Reichardt, M. Pinto, M. Wächtler, M. Stephenson, S. Kupfer, T. Sainuddin, J. Guthmuller, S. A. McFarland, B. Dietzek, *J. Phys. Chem. A*, **2015**, *119*, 3986–3994. DOI: 10.1021/acs.jpca.5b01737
45. C. Reichardt, T. Sainuddin, M. Wächtler, S. Monro, S. Kupfer, J. Guthmuller, S. Gräfe, S. A. McFarland, B. Dietzek, *J. Phys. Chem. A*, **2016**, *120*, 6379–6388. DOI: 10.1021/acs.jpca.6b05957
46. C. Reichardt, K. R. A. Schneider, T. Sainuddin, M. Wächtler, S. A. McFarland, B. Dietzek, *J. Phys. Chem. A*, **2017**, *121*, 5635–5644. DOI: 10.1021/acs.jpca.7b04670
47. A. De la Cadena, D. Davydova, T. Tolstik, C. Reichardt, S. Shukla, D. Akimov, R. Heintzmann, J. Popp, B. Dietzek, *Sci. Rep.*, **2016**, *6*, 33547. DOI: 10.1038/srep33547
48. C. Reichardt, S. Monro, F. H. Sobotta, K. L. Colón, T. Sainuddin, M. Stephenson, E. Sampson, J. Roque III, H. Yin, J. C. Brendel, C. G. Cameron, S. McFarland, B. Dietzek, *Inorg. Chem.*, **2019**, *58*, 3156–3166. DOI: 10.1021/acs.inorgchem.8b03223